Dynamic Article Links ▶

PAPER

Electrochemical and photoelectrochemical investigation of water oxidation with hematite electrodes†

Benjamin Klahr,[a] Sixto Gimenez,[b] Francisco Fabregat-Santiago,[b] Juan Bisquert[b] and Thomas W. Hamann*[a]

Atomic layer deposition (ALD) was utilized to deposit uniform thin films of hematite (α-Fe$_2$O$_3$) on transparent conductive substrates for photocatalytic water oxidation studies. Comparison of the oxidation of water to the oxidation of a fast redox shuttle allowed for new insight in determining the rate limiting processes of water oxidation at hematite electrodes. It was found that an additional overpotential is needed to initiate water oxidation compared to the fast redox shuttle. A combination of electrochemical impedance spectroscopy, photoelectrochemical and electrochemical measurements were employed to determine the cause of the additional overpotential. It was found that photogenerated holes initially oxidize the electrode surface under water oxidation conditions, which is attributed to the first step in water oxidation. A critical number of these surface intermediates need to be generated in order for the subsequent hole-transfer steps to proceed. At higher applied potentials, the behavior of the electrode is virtually identical while oxidizing either water or the fast redox shuttle; the slight discrepancy is attributed to a shift in potential associated with Fermi level pinning by the surface states in the absence of a redox shuttle. A water oxidation mechanism is proposed to interpret these results.

Introduction

Sunlight striking the earth comprises the largest energy resource base currently available.[1] Solar energy is well-distributed across the most populous areas of the globe, making the resource accessible where it is needed most. Further, since it is carbon neutral and environmentally benign, solar energy conversion represents an ideal method of powering the planet. One current drawback of solar energy, however, is that it is diurnal and intermittent, while our energy demands are not. Thus, if the vast solar energy resource is ever to be used to supply a significant fraction of the world's ever-increasing energy demand, efficient methods of storage need to be developed.

Analogous to photosynthesis, storing solar energy in chemical bonds (*i.e.* solar fuels) would be an ideal method. A particularly attractive example of this approach is using solar energy to split water into H$_2$ and O$_2$, where the H$_2$ could subsequently be used in a fuel cell or other energy conversion scheme. Forty years ago,

^{a}*Department of Chemistry, Michigan State University, East Lansing, MI 48824-1322, USA. E-mail: hamann@chemistry.msu.edu*
^{b}*Photovoltaics and Optoelectronic Devices Group, Departament de Física, Universitat Jaume I, 12071 Castelló, Spain*

† Electronic supplementary information (ESI) available. See DOI: 10.1039/c2ee21414h

Broader context

Solar hydrogen production through photoelectrochemical water splitting has the opportunity to supply the world's increasing energy demand with a renewable and transportable fuel. Hematite (α-Fe$_2$O$_3$) has long been considered as a potential candidate for solar water splitting because of a favorable valence band edge position, reasonably low band gap, high stability and low cost. While hematite has a short charge collection length, this issue is being addressed with advances in nanostructuring, which allows for maximizing light absorption while minimizing the distance minority carriers must travel before being collected. A significant overpotential is still required to oxidize water, however, and little is known about the overall water oxidation mechanism at hematite electrodes. This mechanism must be well understood in order to overcome the overpotential and make hematite a practical material for solar hydrogen production. Thin film hematite electrodes were made by atomic layer deposition (ALD) to examine the water oxidation reaction. A suite of photoelectrochemical methods were employed to compare water oxidation to the oxidation of a fast one-electron redox shuttle. These results allowed for an improved understanding of the water oxidation reaction at the hematite electrode surface and the origin of the required overpotential.

the breakthrough report by Fujishima and Honda demonstrated the feasibility of this approach with photo-assisted water splitting on TiO_2 photoelectrodes.[2] Since then, there has been significant effort to develop unassisted water splitting systems. There are several requirements which need to be fulfilled in order to achieve this including good electrode stability in contact with aqueous solutions under harsh conditions and appropriate energetics of the system: the energy of the bottom of the conduction band must be higher than the H^+/H_2 potential and the top of the valence band must be lower in energy than the O_2/OH^- potential.[3] To achieve high efficiency, the additional requirements of good visible light absorption and efficient charge carrier collection must be realized. To date, no single material has fulfilled all the required conditions.[4,5]

Hematite (α-Fe_2O_3) is one promising material for photoelectrochemical (PEC) water splitting which has received a lot of attention due to its combination of sufficiently broad visible light absorption, up to 590 nm, excellent stability under caustic operating conditions and a valence band positioned sufficiently low to oxidize water.[6–8] While hematite's conduction band is too low to reduce water, application of an external bias through a photovoltaic device, or integration of a small bandgap water reduction system in a tandem configuration, would overcome this drawback.[9–11] Despite these favorable characteristics, the water oxidation efficiency at hematite electrodes has been too poor to be commercially viable. One problem is the relatively long visible light absorption depth combined with a very short minority carrier lifetime and mobility, which hinders efficient separation and collection.[12–15] For example, hematite needs to be approximately 375 nm to absorb 95% of incident 550 nm light ($3/\alpha$), whereas the minority carrier collection length is approximately 20 nm.[16–18] This shortcoming has been partially addressed by advances in nanotechnology, where photoelectrodes are able to minimize the charge collection distance while maintaining good light absorption.[19–22]

Thin films serve as excellent model systems for such nanostructured systems since the charge collection dimension can be readily controlled by the film thickness.[16] Further, the uniformity and simple geometry of thin films facilitate the elucidation of the relevant physical properties of hematite photoelectrodes under water splitting conditions. For example, we have recently utilized impedance spectroscopy (IS) to investigate water splitting with hematite thin films.[23] IS is a common tool used in electrochemistry for the analysis of electrical properties of materials and interfaces[24] where a small amplitude AC potential perturbation, $\tilde{V}$, is applied around a constant bias potential. The resulting oscillating current, $\tilde{\imath}$, is measured from which an impedance can be calculated by $Z(\omega) = \tilde{V}/\tilde{\imath}$. Except for materials behaving as a simple resistor, Z includes a real (Z') and imaginary (Z'') component which is represented as a single point for a single frequency. The frequency of the AC signal is typically swept from MHz to mHz to build the impedance spectra Z'' vs. Z' (often termed "Nyquist plots"). The different characteristic times (frequencies) of the processes occurring in the samples (transport, recombination, etc.) can be analyzed independently by using the appropriate electrical model and equivalent circuit. By monitoring the evolution of the relevant resistances and capacitances with the onset of photocurrent we

were able to demonstrate the key role of surface states to water oxidation.[23] Accurate determination of the surface state capacitance, however, requires separation of this capacitance from the bulk capacitance; similar analyses would be problematic with more complicated nanostructures with a non-uniform bulk capacitance. Further, measurements of the bulk capacitance vs. applied potential allowed for determination of the flat-band potential via Mott–Schottky analysis to enable characterization of the system energetics. It is important to note that the Mott–Schottky equation was derived for a planar electrode (e.g. thin film) and is only valid for such electrodes.[25] Since the PEC behavior of hematite electrodes depends strongly on the voltage drop across the depletion region, knowledge of the band edge positions is crucial in interpreting differences in electrode behavior.

While nanostructuring can, in principle, overcome the short minority charge carrier drift-diffusion length, holes that reach the electrode–electrolyte interface must be collected efficiently. We demonstrated on thin films that when fast one-electron redox couples are employed, such as $[Fe(CN)_6]^{3-/4-}$, the hole collection can be quantitative.[17] Similar conclusions were reached by others using a H_2O_2 hole scavenger, although this is a sacrificial agent that also photolytically decomposes during measurements; this drawback prevents stable and reproducible measurements that are time-intensive such as IS.[26] The water oxidation (oxygen evolution) reaction at the hematite electrode surface is generally reported to be sluggish, however, which allows for increased recombination and a concomitant loss in efficiency.[27–32] A detailed understanding of the water oxidation reaction at the hematite electrode surface is therefore very important in devising strategies to overcome this kinetic barrier. There have been several recent studies, employing a variety of techniques, to understand the nature of the slow water splitting reaction with hematite photoelectrodes. For example, Durrant and co-workers used transient absorption (TA) spectroscopy to monitor the evolution of surface-trapped holes and correlated a long trapped hole lifetime with the onset of photocurrent.[29–31,33] One limitation of TA, however, is the difficulty with assigning the energetics of the system, e.g. the position of the relevant surface states. Peter and co-workers recently used IS and intensity modulated photocurrent spectroscopy (IMPS) to study the kinetics of water oxidation at hematite electrodes which also pointed out the crucial role of surface-trapped holes.[27,28,34] We also recently employed IS at different conditions of voltage, light intensity and electrolyte pH to investigate the main steps involved in water oxidation.[23] Importantly, a general physical model, which includes the existence of a surface state at the semiconductor–liquid interface where holes accumulate, was established.

In this work we use atomic layer deposition, ALD, to synthesize thin film hematite photoelectrodes since the unique self-limiting property of ALD results in uniform films with controllable thickness.[35–37] Also, because ALD is not a line-of-sight technique, it can be used to make nanostructured 'thin films' which are prepared in an identical fashion to the model thin films, but have increased light absorption.[38–41] Thus lessons learned with our thin film model system can be directly applied to nanostructured architectures with precisely controlled dimensions fabricated via ALD.[42] We compare the PEC behavior of

hematite with ideally behaving hole collector, $[Fe(CN)_6]^{3-/4-}$, with the behavior under water oxidation conditions. This comparison allows for isolation of the water oxidation steps from the behavior of the bulk hematite electrode. We employed IS and photoelectrochemical measurements to determine the main steps involved in water oxidation. From these combined results we propose a mechanism of water oxidation on hematite electrode surfaces.

Experimental

Thin films of iron oxide were deposited on fluorine-doped tin oxide (FTO) coated glass substrates (Hartford Glass, 12 Ω cm^{-2}) by atomic layer deposition (Savannah 100, Cambridge Nanotech Inc.) using a procedure described previously.[23] Films were prepared by 1200 ALD cycles and measured to be $\sim$60 nm by absorption measurements (Perkin Elmer, Lambda 35 with a Labsphere integrating sphere) corrected for reflection as described previously, as well as ellipsometry measurements (Horiba Jobin Yvon, Smart-SE).[43] Films were determined to be hematite by Raman Spectroscopy and XRD measurements in a previous publication.[16]

Hematite electrodes were masked with a 60 µm Surlyn film (Solaronix) with a 0.25 cm^2 hole to define the active area and to prevent scratching of the thin films. Surlyn films were adhered to the electrodes by heating to 120 °C. The hematite electrodes were examined in contact with aqueous solutions buffered to pH 6.9 using a 0.1 M phosphate buffer, with 200 mM KCl as a supporting electrolyte. The pH was determined with Fisher Scientific Accumet pH meter. Electrolytes containing the $[Fe(CN)_6]^{3-/4-}$ redox couple consisted of 200 mM K$_4$Fe(CN)$_6$ and 20 mM K$_3$Fe(CN)$_6$. The protected hematite electrodes were clamped to a custom made glass electrochemical cell. A homemade saturated Ag/AgCl electrode was used as a reference electrode and high surface area platinum mesh was used as the counter electrode. All potentials were converted to the reversible hydrogen electrode (RHE) scale by the equation $V_{RHE} = V_{Ag/AgCl} + 0.197 + pH(0.059)$. Impedance spectroscopy and photoelectrochemical measurements were made with an Eco Chemie Autolab potentiostat coupled with Nova electrochemical software. Impedance data were gathered using a 10 mV amplitude perturbation of between 10 000 and 0.01 Hz. Data were fit using Zview software (Scribner Associates). The light source was a 450 W Xe arc lamp (Horiba Jobin Yvon). An AM 1.5 solar filter was used to simulate sunlight at 100 mW cm^{-2} (1 sun). Neutral density filters were used to adjust the intensity to 33 mW cm^{-2} (0.33 sun) and 10 mW cm^{-2} (0.1 sun). All photoelectrochemical measurements were performed by shining light on the hematite electrode through the FTO substrate such that there was no competitive light absorption from the electrolyte. Light chopped J–V curves were measured at a rate of 75 mV s^{-1}. The light was chopped using a computer controlled ThorLabs solenoid shutter which was set to activate every 266 ms such that the light was turned on or off every 20 mV. J–V curves were measured at a scan rate of 20 mV s^{-1}. Cyclic voltammogram surface state measurements were performed by applying a potential of 2.0 V vs. RHE under 1 sun illumination for 60 seconds, and then scanning over a potential range in the dark.

Results

J–V curves of a typical thin film hematite electrode immersed in an aqueous electrolyte (H$_2$O) and an aqueous electrolyte containing the $[Fe(CN)_6]^{3-/4-}$ redox couple can be seen in Fig. 1. We have recently shown that the J–V response of hematite thin film electrodes in contact with the $[Fe(CN)_6]^{3-/4-}$ redox couple is limited by the fraction of holes that reach the semiconductor–liquid interface which is determined by the potential drop across the electrode.[15–17] In other words, the surface–hole collection efficiency by $[Fe(CN)_6]^{4-}$ is essentially unity.[15] Since the same film is used in the J–V measurements shown in Fig. 1, in aqueous electrolytes buffered to the same pH under the same illumination conditions, the discrepancy in photocurrent density and onset potential can be attributed to differences in the surface–hole collection efficiency under H$_2$O oxidation conditions (in the absence of a fast hole collector such as $[Fe(CN)_6]^{4-}$). The details underlying this discrepancy are discussed below.

IS measurements were also performed for nominally identical hematite electrodes under the same conditions as the J–V measurements with varying illumination intensities. Nyquist plots resulting from measurements in each electrolyte under 1 sun illumination at 1.3 V vs. RHE and at 1.6 V vs. RHE are displayed in Fig. 2a and b, respectively. At 1.3 V vs. RHE, two clear semicircles are visible for the H$_2$O electrolyte. A full equivalent circuit representing the hematite–liquid junction is shown in Fig. 3a. The equivalent circuit elements include a space-charge capacitance of the bulk hematite, C_{bulk}, surface state capacitance, C_{ss}; the resistances consist of a series resistance, R_S, a resistance which represents the trapping of holes in the surface states, R_{trap}, a charge transfer resistance from the surface states to solution, $R_{ct,ss}$, and a charge transfer resistance from the valence band to solution, $R_{ct,bulk}$. To allow unambiguous fitting of the impedance data to the equivalent circuit in Fig. 3a, $R_{ct,bulk}$ was removed for the case of water oxidation, which yielded the simplified equivalent circuit in Fig. 3b, for reasons that have been discussed elsewhere.[23] At potentials positive of $\sim$1.45 V vs. RHE, the impedance spectra for water oxidation loses the low frequency semicircle and becomes a single semicircle; in this case the simple Randle's circuit, shown in Fig. 3c, is used to fit these impedance spectra. Only one semicircle is visible at all potentials and light conditions measured with the $[Fe(CN)_6]^{3-/4-}$ electrolyte,
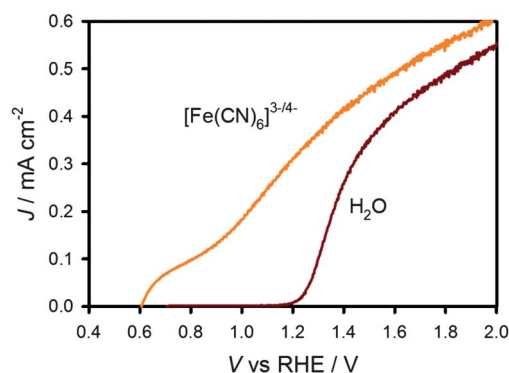
Fig. 1 J–V curve of a hematite electrode in contact with a H$_2$O (red curve) and $[Fe(CN)_6]^{3-/4-}$ (orange curve) electrolyte.

a)

b)
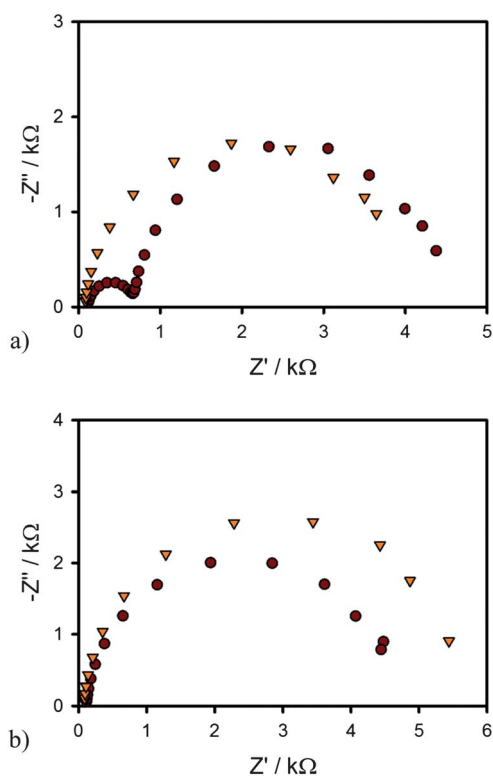
Fig. 2 Nyquist plots for IS data measured under 1 sun illumination for H_2O (red circles) and $[Fe(CN)_6]^{3-/4-}$ (orange triangles) electrolytes at (a) 1.3 V *vs.* RHE and (b) 1.6 V *vs.* RHE.

a)

b)

c)
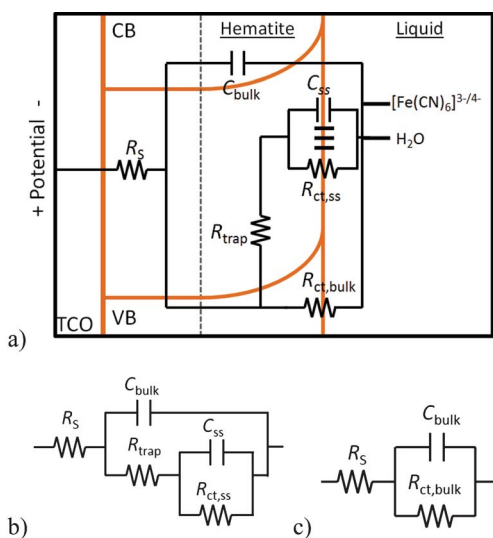
Fig. 3 (a) Full equivalent circuit used to conceptualize hematite–liquid junctions. (b) Simplified model used to fit IS data for Nyquist plots that show 2 semicircles. (c) Simplified model used to fit IS data for Nyquist plots that show 1 semicircle.

therefore a simple Randle's circuit is also used to fit these impedance spectra.

Results from fitting the impedance spectra to the appropriate equivalent circuits described above can be seen in Fig. 4 (additional fitting results are provided in ESI†). Fig. 4a shows a Gaussian distribution of C_{ss} in the H_2O electrolyte, which shifts to more negative potentials with increasing light intensity; this

a)

b)

c)

d)
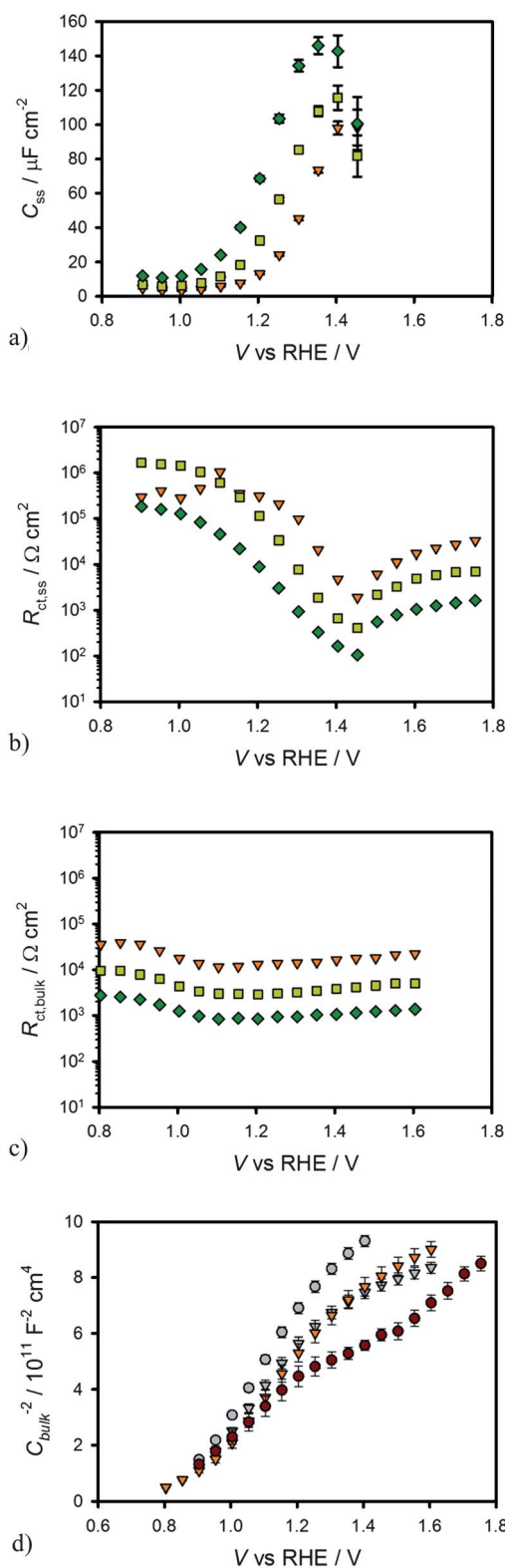
Fig. 4 Equivalent circuit parameters obtained from fitting IS data for a hematite electrode in contact with H_2O (a and b) and $[Fe(CN)_6]^{3-/4-}$ (c) electrolytes under 0.1 sun (orange triangles), 0.33 sun (yellow squares) and 1 sun (green diamonds) illumination. (d) Mott–Schottky plots calculated from C_{bulk} values determined from fitting the impedance spectra for H_2O (circles) and $[Fe(CN)_6]^{3-/4-}$ (triangles) electrolytes in the dark (grey) and under 1 sun illumination (colored).

behavior was described previously.[23] The C_{ss} peak corresponds to a dip in $R_{ct,ss}$ (Fig. 4b), which indicates that interfacial charge transfer (water oxidation) is related to charging of these surface states.[23] With $[Fe(CN)_6]^{3-/4-}$ in solution, however, the charge transfer resistance is essentially constant over the measured potential range for a given light intensity as shown in Fig. 4c. The absence of a measurable surface state capacitance and absence of a dip in the charge transfer resistance suggests that photo-oxidaiton of $[Fe(CN)_6]^{4-}$ does not involve surface states and can be described as a simple outersphere valence band hole collection process. In both electrolytes, there is an obvious decrease of the charge transfer resistance with increasing light intensity which is attributed to a concomitant increase in the number of photo-generated valence band holes with light intensity.

Mott–Schottky plots were created from the derived C_{bulk} values from both H_2O and $[Fe(CN)_6]^{3-/4-}$ electrolytes in the dark and under 1 sun illumination conditions, which are shown in Fig. 4d. The Mott–Schottky plots measured under illumination for water oxidation conditions show a significant horizontal shift compared to the dark, which is an example of Fermi level pinning.[23,44] The Mott–Schottky plots with the $[Fe(CN)_6]^{3-/4-}$ electrolyte are identical in the dark and under illumination, however, further indicating that the surface states do not play a role in $[Fe(CN)_6]^{4-}$ oxidation. In addition, the impedance spectra and Mott–Schottky plots are essentially identical for the H_2O and $[Fe(CN)_6]^{3-/4-}$ electrolytes in the dark, which indicates the surface states are only active under illumination. The details of the surface states are described further below.

The total resistance, R_{tot} was calculated from the IS fittings ($R_{tot} = R_S + R_{trap} + R_{ct,ss}$ for H_2O oxidation and $R_{tot} = R_S + R_{ct,bulk}$ for $[Fe(CN)_6]^{4-}$ oxidation) and was compared to the resistance calculated from the J–V curves where $R_{tot} = dV/dJ$.[23] A plot of R_{tot} calculated from both methods for both H_2O and $[Fe(CN)_6]^{3-/4-}$ electrolytes can be seen in Fig. 5 under 1 sun illumination. The agreement between the calculated R_{tot} from the IS and J–V curves helps to confirm the validity of the equivalent circuit models employed. At potentials negative of the photo-current onset potential for H_2O oxidation, R_{tot} is found to be approximately two orders of magnitude higher compared to R_{tot} for the oxidation of $[Fe(CN)_6]^{4-}$. This large resistance is consistent with the lack of photocurrent density at these potentials. At around 1.2 V, the R_{tot} due to water oxidation drops coincidently with the initiation of photocurrent. Interestingly, R_{tot} for both
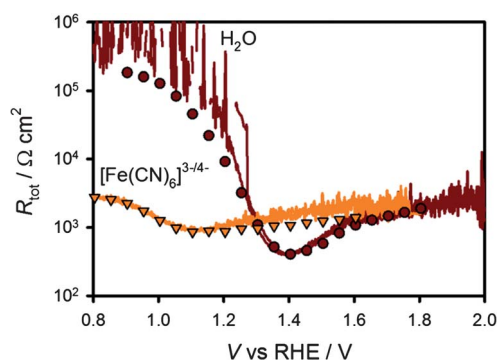
H_2O and $[Fe(CN)_6]^{3-/4-}$ electrolytes become equal at about 1.6 V vs. RHE, suggesting that this hole transfer reaction is not the rate limiting step in water oxidation at positive potentials.

In order to gain further insight into the differences in behavior of hematite electrodes in contact with H_2O and $[Fe(CN)_6]^{3-/4-}$ electrolytes, J–V curves were also measured under light chopping conditions and compared with J–V curves with constant illumination. Fig. 6a shows the superimposed chopped and constant light J–V curves when $[Fe(CN)_6]^{3-/4-}$ is present in the solution. The instantaneous photocurrent density with chopped light reaches the constant light photocurrent density and remains constant until the light is turned off, where the current immediately decays to J_0.[17] This ideal behavior is consistent with the expectations of a fast hole collector efficiently scavenging valence band holes at the surface of a hematite photo-electrode.[15,26,45] In the case of water oxidation, however, the behavior is quite different: see Fig. 6b. At potentials from 0.8–1.2 V vs. RHE, there is a significant instantaneous photocurrent density when the chopped light is turned on, which quickly decays to the near zero steady state photocurrent density under constant illumination. Interestingly, the peak of the H_2O anodic transient photocurrent density closely matches the steady state photocurrent density measured with the $[Fe(CN)_6]^{3-/4-}$ electrolyte (also shown). This is attributed to the identical flux of photogenerated holes which initially reach the surface. When the holes that reach the surface are efficiently collected, as in the case of $[Fe(CN)_6]^{4-}$ oxidation, this flux determines the steady state photocurrent density. Under water oxidation conditions, however, the photocurrent density

a)

b)
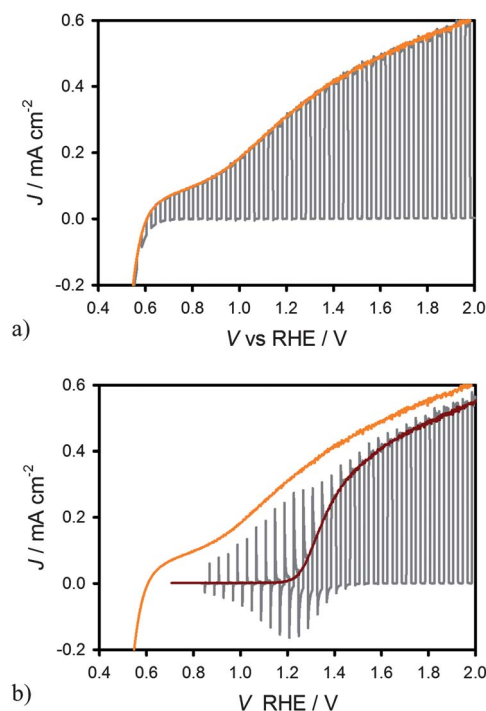
Fig. 6 (a) Chopped light (grey line) and J–V measured under 1 sun illumination (orange line) for a hematite electrode in contact with a $Fe(CN)_6^{3-/4-}$ electrolyte. (b) Chopped light (grey line) and J–V measured under 1 sun illumination (red line) for a hematite electrode in contact with a H_2O electrolyte (the J–V curve measured in a $Fe(CN)_6^{3-/4-}$ electrolyte (orange line) is also shown for comparison).

Fig. 5 R_{tot} calculated from dV/dJ of the J–V curves (lines) and from IS data (symbols) for H_2O and $[Fe(CN)_6]^{3-/4-}$ electrolytes under 1 sun illumination.

decay indicates that a faradaic current cannot be sustained and the hole transfer efficiency is therefore minimal. In this case, the flux of holes that reach the surface must either be trapped in surface states or recombine with conduction band electrons. When the light is switched off at potentials where transient anodic peaks are observed, transient cathodic peaks are also visible. The cathodic transients are thus attributed to reducing the surface-trapped holes. This behavior is consistent with previous reports where current transients were also attributed to the charging and discharging of surface states of α-Fe_2O_3,[32,45,46] CdTe,[47] and TiO_2.[48] Indeed, measuring transient peaks through light chopping has become a prevalent method of qualitatively probing the surface states of hematite.[26,49–53] All additional photogenerated holes, which are not stored in surface states, therefore undergo recombination.

In order to deconvolute the change in potential with change in current over time as in the data shown in Fig. 6, current transients at a constant potential were also measured. These measurements were performed by measuring the current as a function of time at a fixed potential in response to turning on (anodic) and off (cathodic) 1 sun illumination. Plots of the anodic and cathodic current transients measured at various constant potentials can be seen in Fig. 7a and b, respectively. Clearly, there is a dependence in the magnitude of the current transient with potential as well as the rate of decay. In order to determine the amount of charge stored in the surface state at a given potential, the current vs. time plots in Fig. 7 were integrated. A plot of the anodic and cathodic charge stored as

a function of potential is shown in Fig. 8a. The anodic charge was not calculated for potentials above 1.2 V vs. RHE because the faradaic and charging current could not be separated accurately. The cathodic and anodic charge is approximately equal, at least for potentials up to 1.2 V vs. RHE, suggesting that the charge measured is related to the amount of charge trapped in surface states on the hematite electrode. There is a clear peak in the stored charge at approximately 1.3 V vs. RHE. Interestingly, this is near the potential which yields the peak C_{ss} from IS measurements. The same experiments were also performed in response to varying illumination intensities; the results are displayed in Fig. 8b which were calculated from cathodic current

Fig. 7 J measured for a constant V vs. RHE plotted vs. time when 1 sun illumination is turned on (a) and off (b). Time is corrected so that the all of the peaks occur at 10 ms. Measurements are shown for 0.8 V (red solid line), 1.0 V (orange dotted line), 1.2 V (yellow small dashed line), 1.4 V (green dashed dotted line), and 1.6 V (blue large dashed line) vs. RHE.
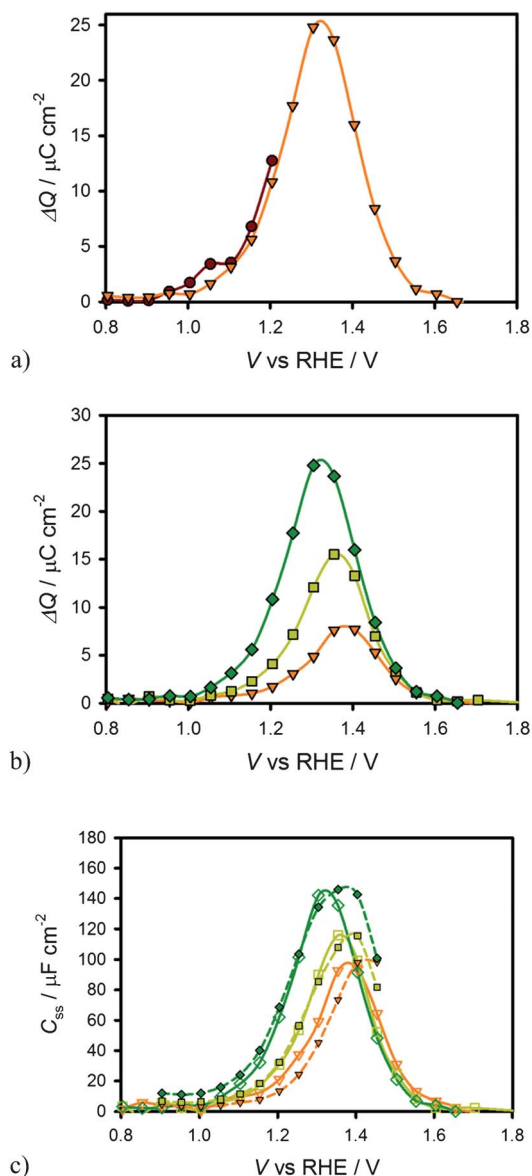
Fig. 8 (a) Transient anodic (red circles) and cathodic (orange triangles) charge passed as a function of potential. (b) Transient cathodic charge vs. potential under 0.1 sun (orange triangles), 0.33 sun (yellow squares) and 1 sun (green diamonds) illumination. (c) C_{ss} determined from IS (open shapes), and C_{ss} determined from current transients (filled in shapes) under 0.1 sun (orange triangles), 0.33 sun (yellow squares) and 1 sun (green diamonds) illumination.

transients. The magnitude of the peak clearly increases with light intensity and the peak shifts to more negative potentials with increasing light intensity. This is the same trend found with the peak of C_{ss} as a function of light intensity measured by IS. The charge measured by the current transients can be related to C_{ss} by the equation $C_{ss} = \Delta Q / \Delta V$ where ΔV is the change in the quasi-Fermi level as a result of turning the light off at a constant potential. Assuming the surface states probed by IS and current transients are the same, ΔV can be calculated by plotting C_{ss} obtained from IS $vs.$ ΔQ measured from current transients (see ESI†). From the slope of these plots, ΔV was found to be 0.08, 0.13 and 0.17 V for 0.1, 0.33 and 1 sun respectively. This corresponds to an increase of 92 mV per 10 fold increase in light intensity, in good agreement with ideal behavior. The C_{ss} calculated from the current transients and IS and can be seen in Fig. 8c. Taken together, these results confirm that the C_{ss} measured with IS is the same entity probed by measuring the stored charge of the current transients.

The potential dependence of the transient photocurrent decay was also examined. Abrantes and Peter examined the decay of current transients of passive iron oxide electrodes in an H_2O electrolyte and were able to gain kinetic insight on the back reaction of electrons reducing surface states (*i.e.* filling surface trapped holes) by fitting the decays to a single exponential function.[45] We found, however, that a double exponential decay is necessary to achieve good fits for the decays measured (see ESI†). Fitting the decays to a double exponential decay function $(\text{Fe(III)} - \text{OH} \underset{e^-}{\overset{h^+}{\rightleftarrows}} \text{Fe(IV)} = \text{O} + \text{H}^+$ where $J(0)$ is the maximum current for the decay process at time $= 0$, τ is the lifetime of the process and $J(\infty)$ is the steady state current reached after both processes have fully decayed) produced two lifetimes that differ by approximately an order of magnitude, which are displayed in Fig. 9. Two lifetimes were also calculated from current transients for both doped and undoped hematite electrodes in water oxidation conditions by Glasscock *et al.*[54] This result is also in reasonable agreement with a recent report by Pendlebury *et al.* of transient absorption spectroscopic measurements on hematite electrodes under water oxidation conditions.[29] Both lifetimes are dependent on potential where the lifetimes increase by approximately an
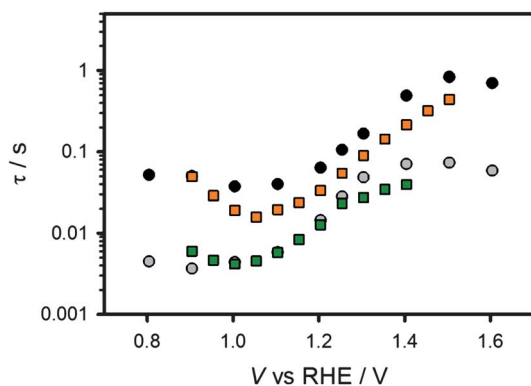
order of magnitude from when there is no faradaic current (1.0 V *vs.* RHE) to when there is significant faradaic current (>1.4 V *vs.* RHE). This also agrees with a recent paper correlating long lived holes and photocurrent on hematite electrodes.[29]

Fig. 9 shows the two lifetimes fit from the double exponential decay of the transients (Fig. 7(b)). The relaxation time of the trapped electrons measured from IS data under 1 sun and 0.1 sun illumination are also shown. It is observed that there is a good match between the fast time constant of the transient discharge time and the relaxation time measured under 1 sun illumination. This suggests that the origin of the two lifetimes found actually results from a single process: the discharging of the surface state. As mentioned above, under illumination, charge is accumulated in the surface state. At short times after switching off the light, the conditions of the surface state (amount of charge accumulated and R_{trap}) are similar as those under illumination. Therefore, the short lifetimes obtained from the transients in Fig. 7b are very close to the relaxation times of the surface state at 1 sun: $\tau_1 \approx (R_S + R_{trap}) \times C_{ss}$. At longer times after switching off the light, the amount of charge in the surface states decreases, mimicking conditions at lower light intensities. Thus, the discharging time rises providing the second, slower process, τ_2, which is consistent with the relaxation time of the surface state obtained at 0.1 sun. The increase in the time constant obtained is due to the increase in R_{trap} during the discharge of the surface state.

The anodic and cathodic current density transients measured above are attributed to the reversible oxidation and reduction, respectively, of surface species. In other words, surface trapping of holes means the photooxidation of a chemical species on the surface (discussed below), and surface recombination is the reduction of that oxidized surface species. We therefore reasoned that we should also be able to measure the surface trapped holes using cyclic voltammetry in the dark. In this experiment, holes accumulate on the surface by applying a positive potential followed by measuring the cathodic current in the dark as the potential is scanned negatively and the surface states are reduced.[55,56] We found, however, that application of a bias required a long holding time at very positive potentials (~2 V *vs.* RHE) to fully oxidize the surface states and obtain reproducible results. We attribute this behavior to hole injection from the substrate to the hematite, which may only occur at very high potentials (when the hematite is fully depleted); thus potentiostatically generated "dark" holes are only present at the hematite surface under these conditions. We therefore also illuminated the electrode while holding it at a positive potential to facilitate the surface state oxidation. A representative experiment measured at 200 mV s^{-1} is shown in Fig. 10a. On the first cycle, shown as a red solid line, a peak in current appears at around 1.3 V and 0.8 V *vs.* RHE. On the second cycle, both of these peaks are gone. The fact that the peaks cannot be seen on the second cycle is consistent with the idea that these peaks represent the reduction of surface trapped holes as the potential is scanned negative on the first cycle. These surface states are not re-oxidized by the application of a positive potential on the relatively fast timescale of this experiment. Thus there is no longer a significant concentration of oxidized surface species to be reduced on the second cycle. The peak at 1.3 V is very close to the peak of C_{ss} fit by the IS data, shown in Fig. 4a, as well as the potential where the maximum

Fig. 9 A plot of the 2 different lifetimes (black and grey circles) fit from a double exponential of the cathodic decays shown in Fig. 7(b). The lifetime of the surface state charging–discharging process at 1 sun (green squares) and at 0.1 sun (orange squares) are also shown.
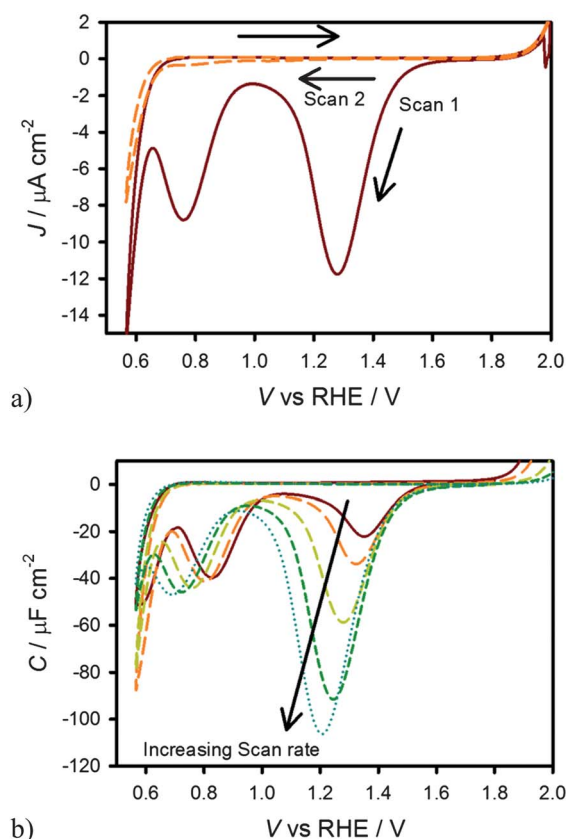
Fig. 10 (a) Cyclic voltammetry of hematite in H_2O scanned at 200 mV s^{-1} after holding the electrode at a potential of 2 V *vs.* RHE for 60 seconds under 1 sun illumination. The first cycle is a solid red line and the second cycle is a dashed orange line. (b) CVs measured with the same conditions as (a) at different scan rates: 20 mV s^{-1} (red, solid), 50 mV s^{-1} (orange, long dash), 200 mV s^{-1} (yellow, medium dash), 500 mV s^{-1} (green, short dash) and 1000 mV s^{-1} (blue, dots).

transient charge is found, shown in Fig. 8. This suggests the peak at 1.3 V is due to filling the surface states which are associated with water oxidation. In order to probe the timescale of the transient peaks, a scan rate dependence of the CV measurements was performed. Capacitance plots were then calculated by dividing the current density by the scan rate, which can be seen in Fig. 10b for varying scan rates. It is apparent that the species probed at 1.3 V *vs.* RHE decreases with scan rate which means the states occupancy decays over time. The time constant(s) of this decay process cannot be confirmed quantitatively because of the constantly changing potential, however the timescale is in general agreement with the transient lifetimes displayed in Fig. 9. This further suggests that the state measured is the same measured in the current transients. The charge passed from the surface states corresponding to the peak at 1.3 V *vs.* RHE was calculated to be 25 μC cm^{-2} when measured at a fast scan rate of 1 V s^{-1}. The similar values between the charge measured through the CV peak, the C_{ss} peak from IS and the charge passed through current transients, as well as the lifetimes measured from the decay of the CV peak and current transients, all suggest that the species being measured around 1.3 V *vs.* RHE is the same for all measurements. Similar CV measurements were also performed

with $[Fe(CN)_6]^{3-/4-}$ in solution (see ESI†) however no cathodic current was measured until the reduction of the $[Fe(CN)_6]^{3-}$ began, again suggesting that the surface states are associated with water oxidation intermediates and not intrinsic to the hematite electrode.

Discussion

The *J*–*V* curves of hematite electrodes immersed in an aqueous electrolyte containing $[Fe(CN)_6]^{3-/4-}$ can be described by the potential dependent fraction of photogenerated holes that reach the electrode surface.[17] These valence band holes at the surface are efficiently collected by $[Fe(CN)_6]^{4-}$, and this faradaic charge transfer results in a steady-state photocurrent density.[15] Under H_2O oxidation conditions the flux of holes to reach the surface (which is just a property of the same bulk semiconductor) is the same, however a steady-state photocurrent is not produced at low applied potentials. Instead of the surface holes undergoing interfacial charge transfer to solution, a fraction of the holes are initially (at low potentials) trapped in surface states; the remainder recombine. This charging of surface states was observed through IS, transient photocurrent and cyclic voltammetric measurements. These results provoke questions regarding the identity of these surface states and their role in the water oxidation process. Instead of being what is generically termed a surface state, we believe the surface states presented herein actually consist of intermediates in the overall water oxidation reaction. One piece of (albeit indirect) evidence of this is that the surface state is only, and always, observed under water oxidation conditions – not in the presence of a competitive hole scavenger. In addition, the surface state at 1.3 V *vs.* RHE is at approximately the same energy as the water oxidation potential (1.23 V *vs.* RHE), which we believe is not just a coincidence.[57]

We therefore propose that the charging of the surface state is actually the first oxidative step in the overall water oxidation reaction. The fully hydroxylated species, $(OH)_3$–Fe–H_3O_3–R where R represents the bulk hematite crystal, is the thermodynamically most stable surface configuration of the (0001) surface.[58] Hellman and Pala recently suggested that the first step of water oxidation on hematite electrodes is the proton coupled oxidation of such surface hydroxide species.[59] This is also in agreement with one of the general mechanisms of water oxidation at metal oxide electrodes previously reviewed by others.[60–62] The initial step is thus given by:

$$J(t) = J(0)_1 e^{-t/\tau_1} + J(0)_2 e^{-t/\tau_2} + J(\infty) \qquad (1)$$

We believe this reaction is what is referred to as "hole trapping" or "surface state charging." Hellman and Pala further calculated that the most stable configuration during water oxidation (at higher applied potentials) is the oxidized $(OH)_3$–Fe–O_3–R surface, also consistent with this assignment.[59] Since the oxidized species on the surface, Fe=O, can be reduced, as demonstrated by the cathodic current transients (Fig. 7) and the CV measurements (Fig. 10), the reaction is written as reversible.

While it is very challenging to directly determine the identity of surface states on a bulk electrode, there are molecular iron catalysts which can serve as analogs. There are several examples of Fe(iv)=O complex intermediates which are known to be involved in catalytic cycles.[63,64] For example, a Fe–TAML

complex was recently shown to catalyze the oxidation of water to dioxygen.[65] Further, Collins and co-workers have shown that the Fe(IV)–oxo species has a reduction potential of 0.9 V vs. NHE in basic conditions, according to the reaction

$$[Fe(IV)L(=O)(OH_2)]^{2-} + e^- + H_2O \rightarrow [Fe(III)L(OH)(OH_2)]^{2-} + OH^- \qquad (2)$$
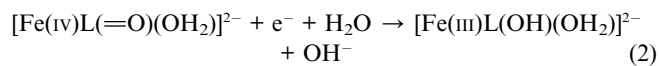
which is essentially the recombination reaction (reduction of the surface intermediate species) proposed herein.[64] This behavior of the Fe(III)–OH/Fe(IV)=O molecular complexes is therefore in good agreement with the proposed first water oxidation step on hematite electrodes. In addition, it was shown that an intermediate Fe(IV)=O complex has a broad absorption spectrum centered at 820 nm.[63] This absorbance is also consistent with the broad near IR absorption observed during water oxidation with hematite electrodes.[29,66]

There are two important features of the surface state behavior that provide further insight into the water oxidation mechanism. The first is that at potentials where the surface oxidation begins, the formation of the proposed intermediate Fe=O does not result in subsequent water oxidation steps as indicated by the lack of steady-state photocurrent; i.e. the transient photocurrent at these potentials decays to zero. Attack of the surface Fe=O by water molecules, leading to a surface bound peroxide followed by decomposition to O_2, should be thermodynamically downhill.[59] In this case, it is expected that the steady-state concentration of surface Fe=O should lead to photocurrent production. Since no photocurrent is observed under these conditions, this is not the predominant mechanism. The other feature is the fact that steady-state concentration of surface Fe=O reaches a peak that is coincident with a sharp drop in the charge transfer resistance and an increase of photocurrent. This indicates that a critical concentration of the surface intermediate species is necessary before further water oxidation steps can proceed. The necessary number of surface intermediates can be estimated by integrating the capacitance as a function of potential. The C_{ss} peaks determined from IS data were fit to a Gaussian curve and integrated to calculate the total charge of the surface states to be 24.3, 31.6 and 38.8 μC cm^{-2} for 0.1, 0.33, and 1 sun illumination respectively. Using the value for 1 sun illumination as an example, this corresponds with a surface coverage of 2.4 × 10^{14} cm^{-2}. The surface coverage is then calculated to be ∼53%, by using the unit cell parameters for the 0001 surface of hematite, and estimating 1 active site per unit cell.[59,67–70] This behavior is consistent with the surface intermediate decomposing bimolecularly, such as:

$$2Fe(IV)=O \rightarrow 2Fe(III) + O_2 \qquad (3)$$
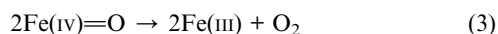
We note that such an oxygen formation mechanism has been proposed extensively before, although not applied to hematite photoelectrodes.[60–62] A water molecule, or hydroxide, could then quickly coordinate to the open iron site to complete the photocatalytic cycle.

At positive potentials ($\geq$1.45 V vs. RHE) the current transients become negligible, the low frequency semicircle disappears from the IS spectra and high steady state photocurrent densities are achieved. This behavior is essentially indistinguishable from when the fast hole collector $[Fe(CN)_6]^{4-}$ is present in solution (Fig. 6b). Further, these two systems have the same charge

transfer resistance at positive potentials. Therefore, the surface hole collection efficiency must also be essentially unity under water oxidation conditions at such positive potentials. Thus, once a sufficient concentration of intermediates are built up, allowing the subsequent steps of water oxidation to proceed, water oxidation is not the rate limiting step in the photoelectrochemical behavior of hematite electrodes; the flux of holes to the electrode surface limits the photocurrent density at these potentials.

We note that the J–V curves of the H_2O and $[Fe(CN)_6]^{3-/4-}$ electrolytes, as seen in Fig. 1, do not overlap exactly, even at positive potentials; the H_2O electrolyte always produces somewhat lower photocurrents at a given positive potential compared to $[Fe(CN)_6]^{3-/4-}$. Since we have demonstrated the surface hole collection efficiency is essentially unity for both of these systems, and the surface hole concentration is determined by the potential drop of the electrode, the discrepancy can be attributed to the extra potential needed to compensate for Fermi level pinning in the H_2O electrolyte. According to the Mott–Schottky plots, the bands under water oxidation are shifted positive compared to $[Fe(CN)_6]^{3-/4-}$. Shifting the J–V curve in the H_2O electrolyte by 200 mV produces excellent agreement with the $[Fe(CN)_6]^{3-/4-}$ J–V curve at positive potentials. A 200 mV shift in band position is also in reasonable agreement with the shift indicated by the Mott–Schottky plot (see ESI†).

Finally, the above discussion of the intrinsic role of the surface state seen at 1.3 V does not include the other state that we observed around 0.8 V in the CV measurements. Since this state's energy is significantly higher than the water oxidation potential, and it is not observed in the impedance spectra at photocurrent onset, we do not think it plays an active role in water oxidation. There are surface terminations of hematite, in addition to the $(OH)_3$–Fe–H_3O_3–R termination discussed above, that are stable. According to Trainor et al., the other most relevant surface is the $(OH)_3$–R termination.[58] This surface can also be oxidized, i.e. trap a hole, but it is thermodynamically uphill for subsequent water oxidation. Importantly, this termination's oxidation potential is approximately 0.5 V more negative than the $(OH)_3$–Fe–H_3O_3–R termination, which is in excellent agreement with the differences in potential of the two surface states we observed.

Conclusion

The photoelectrochemical behavior of hematite electrodes in contact with H_2O and $[Fe(CN)_6]^{3-/4-}$ electrolytes were compared. The photocurrent onset potential was approximately 0.6 V higher in H_2O compared to $[Fe(CN)_6]^{3-/4-}$, which is in accord with literature reports.[15,26,71] The much more positive onset potential represents a loss of energy which must be minimized for any practical use of hematite in water splitting applications. A combination of impedance spectroscopy, photocurrent transient and cyclic voltammetry measurements were therefore employed to determine the cause of the large overpotential for water splitting. We found that at moderate potentials, prior to the photocurrent onset potential, photogenerated holes became trapped in surface states. We deduce that the physical meaning of photogenerated holes being trapped at the surface is that this is the first step in the water oxidation process, specifically the reversible oxidation of surface hydroxide species. It is only after

a buildup of these oxidized intermediates that water oxidation proceeds. It is well known that water oxidation proceeds by an innersphere mechanism, thus a proposed mechanisms should account for this.[62] Describing this reaction exclusively as a charge transfer from a valence band hole is misleading.[72] In addition, the negligible faradaic photocurrent densities at these potentials is often attributed to slow hole transfer kinetics of water oxidation.[27,28,30–32] We suggest that this may be an intrinsic part of the bimolecular mechanism of water oxidation on the hematite surface. At high applied potentials, however, the photocurrent density is essentially the same for the H_2O and $[Fe(CN)_6]^{3-/4-}$ systems; the minor difference is attributed to Fermi level pinning in the H_2O electrolyte. This ideal behavior at high potentials is consistent with the idea that surface state recombination is the process which primarily limits the efficiency of water oxidation at low potentials. Once the surface electron concentration is depleted (by application of a positive potential) a critical concentration of surface intermediates can be formed which leads to efficient subsequent water oxidation. While the addition of catalysts to the electrode surface has been shown to improve the performance, the cause of the improvement has not been established.[33,49,73–76] Insight into the mechanism of water oxidation on hematite, and other surfaces, is critical for the design of better catalysts or other systems aimed at improving the efficiency of water splitting. Work is ongoing in our lab to clarify these points.

Acknowledgements

References

1 *World Energy Assessment Report: Energy and the Challenge of Sustainability*, United Nations Development Program, 2003.
2 A. Fujishima and K. Honda, *Nature*, 1972, **238**, 37.
3 M. G. Walter, E. L. Warren, J. R. McKone, S. W. Boettcher, Q. X. Mi, E. A. Santori and N. S. Lewis, *Chem. Rev.*, 2010, **110**, 6446.
4 J. Bolts and M. Wrighton, *J. Phys. Chem.*, 1976, **80**, 2641.
5 M. A. Butler and D. S. Ginley, *J. Mater. Sci.*, 1980, **15**, 1.
6 J. H. Kennedy and K. W. Frese, *J. Electrochem. Soc.*, 1978, **125**, 709.
7 A. B. Murphy, P. R. F. Barnes, L. K. Randeniya, I. C. Plumb, I. E. Grey, M. D. Horne and J. A. Glasscock, *Int. J. Hydrogen Energy*, 2006, **31**, 1999.
8 L. A. Marusak, R. Messier and W. B. White, *J. Phys. Chem. Solids*, 1980, **41**, 981.
9 A. Duret and M. Gratzel, *J. Phys. Chem. B*, 2005, **109**, 17184.
10 J. Brillet, M. Cornuz, F. Le Formal, J. H. Yum, M. Gratzel and K. Sivula, *J. Mater. Res.*, 2010, **25**, 17.
11 H. L. Wang, T. Deutsch and J. A. Turner, *J. Electrochem. Soc.*, 2008, **155**, F91.
12 R. F. G. Gardner, F. Sweett and D. W. Tanner, *J. Phys. Chem. Solids*, 1963, **24**, 1183.
13 A. G. Joly, J. R. Williams, S. A. Chambers, G. Xiong, W. P. Hess and D. M. Laman, *J. Appl. Phys.*, 2006, **99**, 6.
14 A. J. Bosman and H. J. Vandaal, *Adv. Phys.*, 1970, **19**, 78.
15 B. M. Klahr and T. W. Hamann, *J. Phys. Chem. C*, 2011, **115**, 8393.
16 B. M. Klahr, A. B. F. Martinson and T. W. Hamann, *Langmuir*, 2011, **27**, 461.
17 B. M. Klahr and T. W. Hamann, *Appl. Phys. Lett.*, 2011, **99**, 3.
18 T. W. Hamann, *Dalton Trans.*, 2012, DOI: 10.1039/c2dt30340j.
19 A. Kay, I. Cesar and M. Gratzel, *J. Am. Chem. Soc.*, 2006, **128**, 15714.
20 U. Bjorksten, J. Moser and M. Gratzel, *Chem. Mater.*, 1994, **6**, 858.
21 S. K. Mohapatra, S. E. John, S. Banerjee and M. Misra, *Chem. Mater.*, 2009, **21**, 3048.
22 I. Cesar, K. Sivula, A. Kay, R. Zboril and M. Graetzel, *J. Phys. Chem. C*, 2009, **113**, 772.
23 B. Klahr, S. Gimenez, F. Fabregat-Santiago, J. Bisquert and T. W. Hamann, *J. Am. Chem. Soc.*, 2012, **134**, 4294.
24 A. J. Bard and L. R. Faulkner, *Electrochemical Methods: Fundamentals and Applications*, John Wiley & Sons, New York, 1980.
25 F. Cardon and W. P. Gomes, *J. Phys. D: Appl. Phys.*, 1978, **11**, L63.
26 H. Dotan, K. Sivula, M. Gratzel, A. Rothschild and S. C. Warren, *Energy Environ. Sci.*, 2011, **4**, 958.
27 K. G. Upul Wijayantha, S. Saremi-Yarahmadi and L. M. Peter, *Phys. Chem. Chem. Phys.*, 2011, **13**, 5264.
28 L. M. Peter, K. G. U. Wijayantha and A. A. Tahir, *Faraday Discuss.*, 2012, **155**, 309–322.
29 S. R. Pendlebury, A. J. Cowan, M. Barroso, K. Sivula, J. Ye, M. Gratzel, D. R. Klug, J. Tang and J. R. Durrant, *Energy Environ. Sci.*, 2012, **5**, 6304–6312.
30 S. R. Pendlebury, M. Barroso, A. J. Cowan, K. Sivula, J. W. Tang, M. Gratzel, D. Klug and J. R. Durrant, *Chem. Commun.*, 2011, **47**, 716.
31 A. J. Cowan, C. J. Barnett, S. R. Pendlebury, M. Barroso, K. Sivula, M. Grätzel, J. R. Durrant and D. R. Klug, *J. Am. Chem. Soc.*, 2011, **133**, 10134.
32 M. P. Dareedwards, J. B. Goodenough, A. Hamnett and P. R. Trevellick, *J. Chem. Soc., Faraday Trans. 1*, 1983, **79**, 2027.
33 M. Barroso, A. J. Cowan, S. R. Pendlebury, M. Grätzel, D. R. Klug and J. R. Durrant, *J. Am. Chem. Soc.*, 2011, **133**, 14868.
34 C. Y. Cummings, F. Marken, L. M. Peter, K. G. Upul Wijayantha and A. A. Tahir, *J. Am. Chem. Soc.*, 2011, **134**, 1228–1234.
35 T. W. Hamann, A. B. F. Martinson, J. W. Elam, M. J. Pellin and J. T. Hupp, *J. Phys. Chem. C*, 2008, **112**, 10303.
36 T. W. Hamann, A. B. F. Martinson, J. W. Elam, M. J. Pellin and J. T. Hupp, *Adv. Mater.*, 2008, **20**, 1560.
37 S. M. George, *Chem. Rev.*, 2010, **110**, 111.
38 A. B. F. Martinson, J. W. Elam, J. Liu, M. J. Pellin, T. J. Marks and J. T. Hupp, *Nano Lett.*, 2008, **8**, 2862.
39 Y. Lin, G. Yuan, S. Sheehan, S. Zhou and D. Wang, *Energy Environ. Sci.*, 2011, **4**, 4862.
40 Y. J. Lin, S. Zhou, S. W. Sheehan and D. W. Wang, *J. Am. Chem. Soc.*, 2011, **133**, 2398.
41 Y. Lin, Y. Xu, M. T. Mayer, Z. I. Simpson, G. McMahon, S. Zhou and D. Wang, *J. Am. Chem. Soc.*, 2012, **134**, 5508–5511.
42 M. Rooth, A. Johansson, K. Kukli, J. Aarik, M. Boman and A. Harsta, *Chem. Vap. Deposition*, 2008, **14**, 67.
43 B. M. Klahr, A. B. F. Martinson and T. W. Hamann, *Langmuir*, 2011, **27**, 461.
44 S. R. Morrison, *Electrochemistry at Semiconductor and Oxidized Metal Electrodes*, Plenum, New York, 1980.
45 L. M. Abrantes and L. M. Peter, *J. Electroanal. Chem. Interfacial Electrochem.*, 1983, **150**, 593.
46 K. L. Hardee and A. J. Bard, *J. Electrochem. Soc.*, 1977, **124**, 215.
47 D. Lincot and J. Vedel, *J. Electroanal. Chem.*, 1987, **220**, 179.
48 P. Salvador, *J. Phys. Chem.*, 1985, **89**, 3863.
49 K. J. McDonald and K. S. Choi, *Chem. Mater.*, 2011, **23**, 1686.
50 F. Le Formal, M. Graetzel and K. Sivula, *Adv. Funct. Mater.*, 2010, **20**, 1099.
51 F. Le Formal, N. Tetreault, M. Cornuz, T. Moehl, M. Gratzel and K. Sivula, *Chem. Sci.*, 2011, **2**, 737.
52 K. Sivula, R. Zboril, F. Le Formal, R. Robert, A. Weidenkaff, J. Tucek, J. Frydrych and M. Grätzel, *J. Am. Chem. Soc.*, 2010, **132**, 7436.
53 T. Hisatomi, F. Le Formal, M. Cornuz, J. Brillet, N. Tetreault, K. Sivula and M. Gratzel, *Energy Environ. Sci.*, 2011, **4**, 2512–2515.
54 J. A. Glasscock, P. R. F. Barnes, I. C. Plumb and N. Savvides, *J. Phys. Chem. C*, 2007, **111**, 16477.

55 J. Bisquert, F. Fabregat-Santiago, I. Mora-Sero, G. Garcia-Belmonte, E. M. Barea and E. Palomares, *Inorg. Chim. Acta*, 2008, **361**, 684.

56 G. Boschloo and D. Fitzmaurice, *J. Phys. Chem. B*, 1999, **103**, 2228.

57 B. Klahr, S. Gimenez, F. Fabregat-Santiago, T. Hamann and J. Bisquert, *J. Am. Chem. Soc.*, 2012, **134**, 4294.

58 T. P. Trainor, A. M. Chaka, P. J. Eng, M. Newville, G. A. Waychunas, J. G. Catalano and G. E. Brown, Jr, *Surf. Sci.*, 2004, **573**, 204.

59 A. Hellman and R. G. S. Pala, *J. Phys. Chem. C*, 2011, **115**, 12901.

60 H. Dau, C. Limberg, T. Reier, M. Risch, S. Roggan and P. Strasser, *ChemCatChem*, 2010, **2**, 724.

61 T. R. Cook, D. K. Dogutan, S. Y. Reece, Y. Surendranath, T. S. Teets and D. G. Nocera, *Chem. Rev.*, 2010, **110**, 6474.

62 B. E. Conway and B. V. Tilak, in *Advances in Catalysis*, Academic Press, New York, 1992, vol. 38, p. 1.

63 J.-U. Rohde, J.-H. In, M. H. Lim, W. W. Brennessel, M. R. Bukowski, A. Stubna, E. Münck, W. Nam and L. Que, *Science*, 2003, **299**, 1037.

64 D.-L. Popescu, M. Vrabel, A. Brausam, P. Madsen, G. Lente, I. Fabian, A. D. Ryabov, R. van Eldik and T. J. Collins, *Inorg. Chem.*, 2010, **49**, 11439.

65 W. C. Ellis, N. D. McDaniel, S. Bernhard and T. J. Collins, *J. Am. Chem. Soc.*, 2010, **132**, 10990.

66 C. Y. Cummings, F. Marken, L. M. Peter, K. G. Upul Wijayantha and A. A. Tahir, *J. Am. Chem. Soc.*, 2011, **134**, 1228.

67 R. L. Blake and R. E. Hessevick, *Am. Mineral.*, 1966, **51**, 123.

68 C. M. Eggleston and M. F. Hochella, *Am. Mineral.*, 1992, **77**, 911.

69 C. M. Eggleston, A. G. Stack, K. M. Rosso, S. R. Higgins, A. M. Bice, S. W. Boese, R. D. Pribyl and J. J. Nichols, *Geochim. Cosmochim. Acta*, 2003, **67**, 985.

70 The number of active sites per unit cell is estimated by assuming one Fe atom in a given plane per unit cell. Each atom is estimated to have only 1 active site because the formation of 2 oxo groups on a single Fe atom is energetically unfavorable.

71 H. L. Sanchez, H. Steinfink and H. S. White, *J. Solid State Chem.*, 1982, **41**, 90.

72 A. J. Bard, *J. Am. Chem. Soc.*, 2010, **132**, 7559.

73 D. K. Zhong, M. Cornuz, K. Sivula, M. Graetzel and D. R. Gamelin, *Energy Environ. Sci.*, 2011, **4**, 1759.

74 C. Y. Cummings, F. Marken, L. M. Peter, A. A. Tahir and K. G. U. Wijayantha, *Chem. Commun.*, 2012, **48**, 2027–2029.

75 D. K. Zhong and D. R. Gamelin, *J. Am. Chem. Soc.*, 2010, **132**, 4202.

76 D. K. Zhong, J. W. Sun, H. Inumaru and D. R. Gamelin, *J. Am. Chem. Soc.*, 2009, **131**, 6086.